Origin of DC and AC conductivity anisotropy in iron-based superconductors: Scattering rate versus spectral weight effects

Michael Schütt,[1] Jörg Schmalian,[2] and Rafael M. Fernandes[1]

[1]*School of Physics and Astronomy, University of Minnesota, Minneapolis 55455, USA*

[2]*Institute for Theory of Condensed Matter and Institute for Solid State Physics, Karlsruhe Institute of Technology, 76128 Karlsruhe, Germany*

(Received 8 December 2015; revised manuscript received 19 July 2016; published 8 August 2016)

To shed light on the transport properties of electronic nematic phases, we investigate the anisotropic properties of the AC and DC conductivities. Based on the analytical properties of the former, we show that the anisotropy of the effective scattering rate behaves differently than the actual scattering rate anisotropy and even changes sign as a function of temperature. Similarly, the effective spectral weight acquires an anisotropy even when the plasma frequency is isotropic. These results are illustrated by an explicit calculation of the AC conductivity due to the interaction between electrons and spin fluctuations in the nematic phase of the iron-based superconductors and shown to be in agreement with recent experiments.

DOI: 10.1103/PhysRevB.94.075111

In-plane resistivity anisotropy measurements have been employed as the primary tool to investigate the nematic phase of both cuprate and iron-based superconductors [1–5]. In these systems, the onset of electronic nematic order, characterized by an Ising order parameter $\varphi \neq 0$, lowers the point-group symmetry from tetragonal to orthorhombic, making the two in-plane x and y directions inequivalent [6–8]. As a result, a nonzero conductivity anisotropy arises, $\Delta\sigma = \sigma_x - \sigma_y \neq 0$ [9].

In general, the longitudinal DC conductivity along direction $\mu = x, y$ can be expressed in terms of the Drude form $\sigma_\mu = \tau_\mu \Omega_{p,\mu}^2/(4\pi)$, where τ_μ^{-1} is the transport scattering rate and $\Omega_{p,\mu}$ is the plasma frequency. Therefore, an anisotropy in the DC conductivity can arise from an anisotropic scattering rate, which is sensitive to impurities and low-energy excitations of the system, and/or from an anisotropic Drude weight, which is sensitive to the electronic structure. In the nematic phase of the iron-based superconductors, different effects contribute to these quantities. Anisotropic magnetic fluctuations triggered by nematic order [10,11] give rise to an anisotropy in the inelastic scattering rate [12–14], whereas the dressing of an impurity potential by magnetic correlations promotes an anisotropy in the elastic scattering rate [15,16]. Conversely, the distortion of the Fermi surface caused by the ferro-orbital order triggered at the nematic transition affects the plasma frequency [17–20]. Disentangling these contributions would provide important insight into the dominant sources of anisotropy in the nematic phase. Furthermore, it would offer important benchmarks to test theories proposed to explain the nematic instability—particularly of the hotly debated compound FeSe, where a variety of scenarios have been proposed, such as magnetic fluctuations [21,22], charge-current fluctuations [23], a Pomeranchuk instability [24,25], and different types of orbital order [26].

At first sight, a natural way to disentangle τ_μ^{-1} and $\Omega_{p,\mu}$ is via the width and the area of the Drude peak of the AC conductivity, $\sigma_\mu(\omega)$. In this paper, however, we show that these quantities are unavoidably entangled. This general result follows directly from the memory function formalism, which is valid even in the absence of quasiparticles, and yields the following form for the AC conductivity [27]:

$$\sigma_\mu(\omega) = \frac{\Omega_{p,\mu}^2}{4\pi} \frac{1}{\tau_\mu^{-1}(\omega) - i\omega[1 + \lambda_\mu(\omega)]}. \tag{1}$$

The main point is that, besides $\Omega_{p,\mu}$ and τ_μ^{-1}, the AC conductivity depends on the optical mass enhancement λ_μ [28]. While λ_μ does not contribute to the DC conductivity $\sigma_\mu(\omega \to 0)$, it does modify the *effective* plasma frequency $\tilde{\Omega}_{p,\mu}^2$ (as extracted from the area of the Drude peak) and the *effective* scattering rate $\tilde{\tau}_\mu^{-1}$ (as extracted from the width of the Drude peak), yielding $\tilde{\Omega}_{p,\mu}^2 = \Omega_{p,\mu}^2/(1 + \lambda_\mu)$ and $\tilde{\tau}_\mu^{-1} = \tau_\mu^{-1}/(1 + \lambda_\mu)$. Consequently, the effective scattering rate anisotropy depends on both the actual scattering rate anisotropy $\Delta\tau^{-1} \equiv \tau_x^{-1} - \tau_y^{-1}$ and the optical mass anisotropy $\Delta\lambda \equiv \lambda_x - \lambda_y$ via $\Delta\tilde{\tau}^{-1} = \Delta\tau^{-1} - \tau_0^{-1}\Delta\lambda$, where we assume the impurity induced scattering rate τ_0^{-1} to be isotropic. The DC conductivity anisotropy, in contrast, is sensitive only to $\Delta\tau^{-1}$. Because of the analytical properties of the AC conductivity, $\Delta\tau^{-1}$ and $\Delta\lambda$ are related by a Kramers-Kronig transformation, which very generally enforces the same sign upon them [see Supplemental Material (Ref. [41])]. As a result, $\Delta\tilde{\tau}^{-1}$ is suppressed with respect to $\Delta\tau^{-1}$. Even more, because inelastic scattering is suppressed as temperature is lowered, the effective scattering rate anisotropy can change sign as a function of temperature, while the DC conductivity anisotropy retains the same sign. Analogously, the effective plasma frequency can acquire an anisotropy even if the actual plasma frequency is isotropic, since $\Delta\tilde{\Omega}_p^2 = -\Omega_{p,0}^2\Delta\lambda$.

These general results strongly impact the interpretation of transport data in nematic phases. To highlight their importance, we refer to recent measurements of $\Delta\sigma(\omega)$ in detwinned $BaFe_2As_2$, which reported a larger anisotropy in the effective plasma frequency than in the effective scattering rate [4,29]. In Fig. 1 we plot $\mathrm{Re}[\sigma_\mu(\omega)]$ in Eq. (1) considering four cases: (i) anisotropy only in the plasma frequency ($\Omega_{p,y} < \Omega_{p,x}$); (ii) anisotropy only in the scattering rate ($\tau_y^{-1} > \tau_x^{-1}$); (iii) anisotropy only in the optical mass ($\lambda_y > \lambda_x$); (iv) anisotropy in both scattering rate and optical mass ($\tau_y^{-1} > \tau_x^{-1}$ and

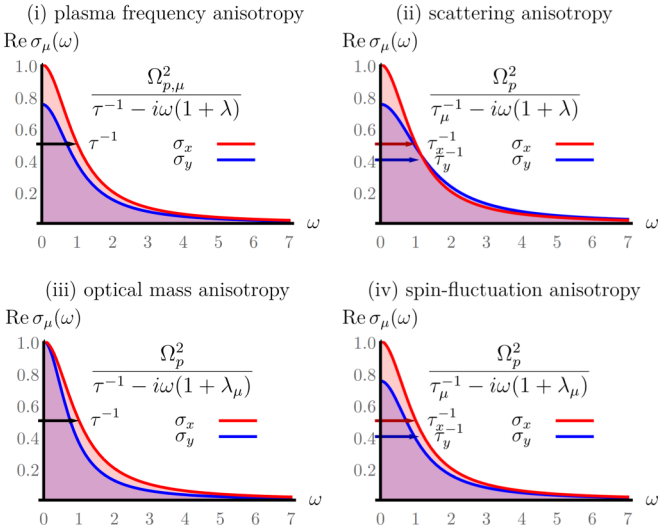

FIG. 1. AC conductivity $\sigma_\mu(\omega)$ of Eq. (1) as a function of frequency ω for both x and y directions. In case (i), only the plasma frequency is anisotropic $[\Omega^2_{p,y} = (3/4)\Omega^2_{p,x}]$, while in (ii) and (iii) only the scattering rate $[\tau_y^{-1} = (4/3)\tau_x^{-1}]$ and the optical mass $[\lambda_y = (4/3)\lambda_x]$ are anisotropic, respectively. Panel (iv) shows the case in which both the scattering rate and the optical mass are anisotropic, yielding AC and DC conductivities very similar to those in panel (i). The causality properties of the AC conductivity do not allow cases (ii) and (iii) to exist, i.e., both τ_μ^{-1} and λ_μ must be present.

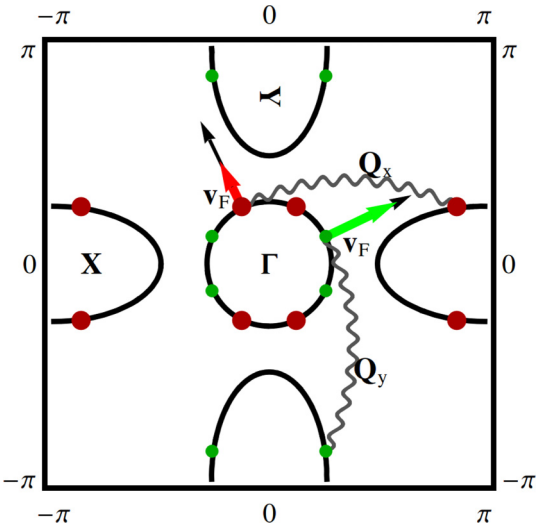

FIG. 2. Illustration of the Fermi surface, consisting of holelike (at Γ) and electronlike pockets (at X and Y), and the anisotropic processes promoted by spin fluctuations. On one hand, scattering off of spin fluctuations is stronger for the hot spots exchanging $\mathbf{Q}_X = (\pi,0)$ (red dots) than $\mathbf{Q}_Y = (0,\pi)$ (green dots) fluctuations. On the other hand, the renormalized Fermi velocity suppression (or, equivalently, mass renormalization) caused by the exchange of spin fluctuations (arrows) is larger at the red hot spots than at the green hot spots.

$\lambda_y > \lambda_x$). The system in cases (i) and (ii) have very similar DC conductivities but different AC conductivities in the intermediate frequency range. In the presence of an optical mass anisotropy only, case (iii), the system does not display a DC conductivity anisotropy, instead the intermediate frequency range is similar to that of case (i). The key point is that cases (ii) and (iii) are not allowed due to the causality properties of the AC conductivity, which require *both* τ_μ^{-1} and λ_μ to be present. After combining these two effects, case (iv), the system displays DC and AC conductivities very similar to case (i). Thus, the AC conductivity anisotropy observed in Refs. [4,29] is equally consistent with either case (i) or (iv), which have very different physical origins—electronic-structure anisotropy and scattering rate anisotropy, respectively.

To illustrate our results, we explicitly compute the AC conductivity of a multiband model for the iron pnictides in which the electrons interact with spin fluctuations, which become anisotropic in the nematic phase [10,11]. While this interaction does not promote anisotropy in the bare plasma frequency ($\Delta\Omega_p = 0$), it causes $\Delta\tau^{-1} \neq 0$ and $\Delta\lambda \neq 0$ with the same relative sign. Physically, the first effect arises from real collisions of electrons and magnetic fluctuations, whereas the latter effect stems from the reduction of the electronic Fermi velocity (or, equivalently, the enhancement of the effective electron mass) promoted by the exchange of virtual spin fluctuations (see Fig. 2). Interestingly, because collisions are suppressed at low temperatures, $\Delta\tau^{-1}$ decreases as the temperature is lowered. In contrast, $\Delta\lambda$ remains finite as $T \to 0$, since it is proportional to the electronic mass renormalization. Consequently, one generally expects a sign change of $\Delta\tilde{\tau}^{-1} = \Delta\tau^{-1} - \tau_0^{-1}\Delta\lambda$ as a function of temperature, accompanied by an increase in $\Delta\tilde{\Omega}^2_p = -\Omega^2_{p,0}\Delta\lambda$, despite the fact that $\Delta\sigma(\omega \to 0) \propto \Delta\tau^{-1}$ retains the same sign. These behaviors agree with the AC conductivity measurements in detwinned $BaFe_2As_2$ [4,29]. We note that anisotropies in the electronic structure, not considered here, will generically cause anisotropy in Ω_p but not in τ^{-1} or λ.

Our starting point is the minimal three-band model shown in Fig. 2 [30], and previously employed to investigate the DC conductivity anisotropy due to the scattering by spin fluctuations [12]. This model has a holelike circular pocket centered at the $\Gamma = (0,0)$ point of the Fe-square lattice Brillouin zone, and two elliptical electron pockets centered at $X = (\pi,0)$ and $Y = (0,\pi)$. Hereafter, for convenience, these bands are labeled $\beta = 0$, $\beta = 1$, and $\beta = -1$, respectively. We also include in the model pointlike impurities, giving rise to the isotropic band-independent elastic scattering rate τ_0^{-1}. We emphasize that our goal here is not to provide a quantitative fitting to the AC conductivity data, which requires detailed electronic structure calculations [31–35], but rather to illustrate the general properties of $\Delta\sigma(\omega)$ discussed above.

In our problem, the AC conductivity can be written in a band-resolved manner, $\sigma_\mu = \sum_\beta \sigma_\mu^\beta$. Without interactions, we have $\sigma^\beta_{0,\mu} = \frac{1}{4\pi}(\Omega^\beta_{p,\mu})^2/(\tau_0^{-1} - i\omega)$, where the subscript 0 denotes the noninteracting system and $\Omega^\beta_{p,\mu} = \sqrt{\frac{2e^2 N_F^\beta}{\hbar}} v_F^\beta$, with density of states N_F^β and averaged Fermi velocity v_F^β. The tetragonal symmetry of the system implies $\Omega^\beta_{p,x} = \Omega^{-\beta}_{p,y}$, i.e., $\sigma^\beta_{0,x} = \sigma^{-\beta}_{0,y}$, yielding $\Delta\sigma_0 \equiv \sigma_{0,x} - \sigma_{0,y} = 0$, as expected for a tetragonal system.

The contribution arising from the interaction with spin fluctuations is conveniently expressed in terms of the memory function $M^\beta_\mu(\omega)$, defined such that

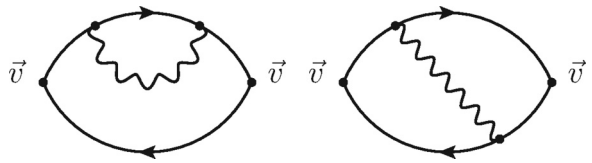

FIG. 3. Interaction corrections to the optical conductivity diagrams: self-energy Φ^{self} (left) and vertex corrections Φ^{vert} (right). Solid lines refer to the electronic propagator, wavy lines denote the spin fluctuation propagator, and $\mathbf{v}$ is the velocity vertex.

$\sigma_\mu^\beta = \frac{1}{4\pi}(\Omega_{p,\mu}^\beta)^2/[\tau_0^{-1} - i\omega + M_\mu^\beta(\omega)]$ [27]. Hence, while $\mathrm{Re}(M_\mu^\beta)$ renormalizes the scattering rate, $-\mathrm{Im}(M_\mu^\beta)/\omega$ renormalizes the optical mass. The fact that these two quantities are related by Kramers-Kronig relations implies that an anisotropy in the scattering rate must be accompanied by an anisotropy in the optical mass, as stated in the introduction. In this framework, calculating the band-resolved AC conductivity anisotropy, $\Delta\sigma^\beta \equiv \sigma_x^\beta - \sigma_y^{-\beta}$, is equivalent to calculating the anisotropic memory function $\Delta M^\beta = M_x^\beta - M_y^{-\beta}$, since $\Delta\sigma^\beta = -(\frac{\sigma_{0,x}^\beta}{\tau_0^{-1}-i\omega})\Delta M^\beta$. Consequently, expansion of ΔM^β for small frequencies yields the anisotropic scattering rate and optical mass, $\Delta M^\beta = (\Delta\tau^\beta)^{-1} - i\omega\Delta\lambda^\beta$.

To leading order in the interaction parameter g between the electrons and the spin fluctuations, the memory function is given by the two Feynman diagrams depicted in Fig. 3 [36], where solid lines denote the electronic Green's function $\mathcal{G}_k^\beta = (i\tilde{\omega}_n - \epsilon_{\mathbf{k}}^\beta)^{-1}$ and the wavy lines denote the spin fluctuation dynamic susceptibility χ_k. Here, $k = (i\omega_n, \mathbf{k})$ is both momentum $\mathbf{k}$ and Matsubara frequency ω_n, $\epsilon_{\mathbf{k}}^\beta \approx \mathbf{v}_F^\beta \cdot \mathbf{k}$ is the linearized dispersion of band β, and $\tilde{\omega}_n = \omega_n + \mathrm{sgn}(\omega_n)/(2\tau_0)$ incorporates the effect of impurity scattering within the Born approximation. In particular, the memory function is given by the combination of $(\frac{\sigma_{0,\mu}^\beta}{\tau_0^{-1}-i\omega})M_\mu^\beta = \frac{e^2}{i\omega}(2\Phi_\mu^{\text{self},\beta} + \Phi_\mu^{\text{vert},\beta})$ with:

$$\Phi_{\mu,p}^{\text{self},\beta} = g^2 \sum_{\beta'} \int_{k,k'} \chi_{k-k'}^{(\beta\beta')} \mathcal{G}_k^\beta v_{\mu,k}^\beta \mathcal{G}_{k+p}^\beta \mathcal{G}_{k'+p}^{\beta'} \mathcal{G}_{k+p}^\beta v_{\mu,k+p}^\beta, \quad (2)$$

$$\Phi_{\mu,p}^{\text{vert},\beta} = g^2 \sum_{\beta'} \int_{k,k'} \chi_{k-k'}^{(\beta\beta')} \mathcal{G}_k^\beta v_{\mu,k}^\beta \mathcal{G}_{k+p}^\lambda \mathcal{G}_{k'}^{\beta'} v_{\mu,k'+p}^{\beta'} \mathcal{G}_{k'+p}^{\beta'}, \quad (3)$$

where $v_{\mu,k}^\beta$ is the velocity, $p = (i\Omega_n, 0)$, and $\int_k = T\sum_{\omega_n}\int_{\text{BZ}} \mathrm{d}^2k/(2\pi)^2$. As shown by inelastic neutron scattering data [37], the magnetic susceptibility is peaked at the ordering vectors $\mathbf{Q}_X = (\pi, 0)$ and $\mathbf{Q}_Y = (0, \pi)$. Therefore, only the terms $\chi_k^{(10)} \equiv \chi_{X,k}$ and $\chi_k^{(-10)} \equiv \chi_{Y,k}$ contribute. At low energies and in the tetragonal phase, these susceptibilities are equal and described by $\chi_{j,k}^{-1} = \chi_0^{-1}(\xi^{-2} + |\mathbf{k} - \mathbf{Q}_j|^2 + |\omega_n|/\gamma)$, where χ_0^{-1} is the magnetic energy scale, ξ is the correlation length (in units of the lattice constant), and γ is the Landau damping. Indeed, this form has been widely used to fit the neutron data in pnictides [37–39]. In the nematic phase, the susceptibilities become different, since magnetic fluctuations become stronger along either $\mathbf{Q}_X$ or $\mathbf{Q}_Y$. Specifically, the correlation lengths are renormalized by the nematic order parameter φ, yielding $\chi_{j,k}^{-1} = \chi_{j,k}^{-1} \mp \chi_0^{-1}\xi^{-2}\varphi$ [10].

Such an anisotropy in the spin fluctuation spectrum, which is observed experimentally [11], controls the memory function anisotropy. Consequently, it is useful to expand ΔM^β for small φ. In contrast to the isotropic part of the memory function [40], the behavior of ΔM^β is dominated by the hot spots, i.e., points of the Fermi surface connected by the magnetic ordering vectors $\mathbf{Q}_X = (\pi, 0)$ and $\mathbf{Q}_Y = (0, \pi)$, $\epsilon_{\mathbf{k}}^\beta = \epsilon_{\mathbf{k}+\mathbf{Q}_j}^{\beta'}$ (see Fig. 2). Focusing on this contribution, we find the analytical expression:

$$\Delta M^\beta(\omega) = -\varphi\tilde{g}^2 C_{\text{eff}}^\beta \omega\, \mathcal{K}\left(\frac{\xi^{-2}}{2\pi}\frac{\gamma}{T}, \frac{\omega}{\xi^{-2}\gamma}\right). \quad (4)$$

where we defined the dimensionless coupling constant $\tilde{g}^2 = g^2\chi_0\nu_F^\beta$ and the complex function:

$$\mathcal{K}(s,t) = -\frac{1}{t}\left[1 - \frac{1}{2s} + \left(1 + \frac{i}{t}\right) \times \left(\frac{1}{s} + \psi(s) - \psi(1 + s - ist)\right)\right], \quad (5)$$

with ψ denoting the digamma function. Equation (4) naturally separates the contributions arising from the Fermi surface geometry, into C_{eff}^β (see Supplemental Material [41] for the full expression), and the contributions arising from the spin dynamics, encoded in $\mathcal{K}(s,t)$ via the two dimensionless parameters $s \equiv \xi^{-2}\gamma/(2\pi T)$ and $t \equiv \omega/(\xi^{-2}\gamma)$. While s depends on the ratio between the spin correlation length ξ and the length of thermal spin fluctuations $\xi_T^2 \equiv \gamma/T$, t depends explicitly on the frequency. Because we are interested in the interaction-induced corrections to the Drude formula, hereafter we take the limit $t \ll 1$. Terms beyond this approximation are particularly important near quantum critical points, where $\xi \to \infty$, and at frequencies larger than the scale set by the isotropic scattering rate τ_0^{-1}, which is of the order of 300 meV in $BaFe_2As_2$ [see Supplemental Material (Ref. [41]) and also Ref. [42]]. Although the study of these contributions is beyond the scope of this paper, we note that for $\omega \gg \tau_0^{-1}$ they give rise to a slower decay of $\mathrm{Re}[\sigma(\omega)]$ than the standard ω^{-2} Drude behavior [43].

In terms of the function $\mathcal{K}(s,t)$, the anisotropies in the bare scattering rate and in the optical mass are given by $(\Delta\tau^\beta)^{-1} = -\varphi\tilde{g}^2 C_{\text{eff}}^\beta \omega\, \mathrm{Re}\,\mathcal{K}(s, t \to 0)$ and $\Delta\lambda^\beta = \varphi\tilde{g}^2 C_{\text{eff}}^\beta\, \mathrm{Im}\,\mathcal{K}(s,0)$, yielding the effective scattering rate and plasma frequency anisotropies:

$$(\Delta\tilde{\tau}^\beta)^{-1} = -\varphi g'^2 C_{\text{eff}}^\beta\left[\omega\,\mathrm{Re}\,\mathcal{K}(s, t \to 0) + \tau_0^{-1}\,\mathrm{Im}\,\mathcal{K}(s,0)\right]$$
$$\left(\Delta\tilde{\Omega}_p^\beta\right)^2 = -\varphi\tilde{g}^2 C_{\text{eff}}^\beta \left(\Omega_{p,x}^\beta\right)^2 \mathrm{Im}\,\mathcal{K}(s,0). \quad (6)$$

As can be confirmed by explicit evaluation of Eq. (5), the analytical properties of the complex function $\mathcal{K}(s,t)$ enforce its real part to be positive and its imaginary part to be negative. This is due to the origin of the former from collisions of electrons by spin fluctuations—the same process that causes a electronic lifetime via the imaginary part of the self-energy, whereas the latter arises from the suppression of the electronic Fermi velocity—the same process that enhances the electronic mass via the real part of the self-energy (see Fig. 1). Consequently, the two contributions to $(\Delta\tilde{\tau}^\beta)^{-1}$ in Eq. (6) have opposite signs, resulting in a suppression of the effective

scattering rate compared to the bare scattering rate $(\Delta\tau^{\beta})^{-1}$. Furthermore, because of their different physical origins—inelastic collision *versus* Fermi velocity renormalization—the two contributions to the effective scattering rate $(\Delta\tilde{\tau}^{\beta})^{-1}$ display a different temperature dependency. Using Eq. (5), we find that at high temperatures ($T \gg \gamma\xi^{-2}$) the behaviors $\omega\,\mathrm{Re}\,\mathcal{K}(s,0^{+}) \propto T$ and $\mathrm{Im}\,\mathcal{K}(s,0) \propto -\frac{1}{T}$, whereas at low temperatures ($T \ll \gamma\xi^{-2}$) we have $\omega\,\mathrm{Re}\,\mathcal{K}(s,0^{+}) \propto T^{2}$ and $\mathrm{Im}\,\mathcal{K}(s,0) = -\frac{1}{2}$. Thus, while $\mathrm{Re}\,\mathcal{K} > 0$ dominates the high-temperature regime, $\mathrm{Im}\,\mathcal{K} < 0$ governs the low-temperature regime. This can be physically understood from the fact that $\mathrm{Re}\,\mathcal{K}$ arises from the collision between electrons and spin fluctuations, which are completely suppressed at $T = 0$, whereas $\mathrm{Im}\,\mathcal{K}$ arises from the suppression of the Fermi velocity, which persists down to $T = 0$.

Therefore, one expects that as temperature is lowered, the anisotropy of the effective scattering rate changes sign. Using characteristic values for $BaFe_2As_2$ [see Supplemental Material (Ref. [41]) and also Ref. [42]], $\tau_0^{-1} \sim 300$ meV from the residual resistivity and $\gamma \sim 100$ meV, $\xi \sim 5a$ from neutron scattering [39], we find that the two contributions become comparable at the temperature scale $T^{*} \sim 100$ K. Interestingly, recent optical conductivity data in this compound [29] find such a behavior, with $(\Delta\tilde{\tau}^{\beta})^{-1}$ changing sign below the nematic transition at $T_{\mathrm{nem}} \sim 150$ K. Although these compounds also display long-range magnetic order, at these temperatures the resulting reconstruction of the Fermi surface is incipient [44], suggesting that the mechanism discussed here could be at play.

We emphasize that the sign change in the effective scattering rate $(\Delta\tilde{\tau}^{\beta})^{-1}$ does not cause a sign change in the DC conductivity anisotropy—also in agreement with the experiments. Indeed, as is clear from Eq. (1), the DC conductivity anisotropy depends only on the bare scattering rate $(\Delta\tau^{\beta})^{-1}$, which in turn is solely determined by $\mathrm{Re}\,\mathcal{K}$, $\Delta\sigma(\omega = 0) = -\frac{1}{4\pi}\sum_{\beta}(\Omega^{\beta}_{0,x})^{2}\tau_0^{2}(\Delta\tau^{\beta})^{-1}$. The main consequence of the reduction of the effective scattering rate $(\Delta\tilde{\tau}^{\beta})^{-1}$ is an accompanying enhancement of the anisotropic Drude spectral weight $\Delta\mathrm{SW} \equiv \int_0^{\infty}\Delta\sigma(\omega)d\omega$, since $\Delta\mathrm{SW} = \frac{1}{8}\sum_{\beta}(\Delta\tilde{\Omega}^{\beta}_{p})^{2}$ depends only on $\mathrm{Im}\,\mathcal{K}$, as shown in Eq. (6). This means that any suppression of the effective scattering rate is compensated by an enhancement of the effective Drude weight, keeping the DC anisotropy the same.

The global sign of $\Delta\sigma(\omega = 0)$ and $\Delta\mathrm{SW}$ depend on the same parameters C^{β}_{eff} via Eq. (6), which are determined by the Fermi surface geometry. We calculate them explicitly in Fig. 4 for a toy model in which the hole pocket is a circle, $\epsilon_{\Gamma} = \epsilon_0 - \frac{\mathbf{p}^2}{2m}$, whereas the electron pockets are ellipses, $\epsilon_{X/Y} = \frac{p_x^2}{2m(1\pm\delta)} + \frac{p_y^2}{2m(1\mp\delta)} - \epsilon_0$ [12,45]. By fixing the ellipticity δ, we find that in general the weighted sum of C^{β}_{eff} is positive for electron-doped compounds ($\mu > 0$) and negative for hole-doped compounds ($\mu < 0$). Consequently, because $\varphi > 0$ for a detwinned sample with tensile strain applied along the x direction [11], we find $\Delta\sigma > 0$ and $\Delta\mathrm{SW} > 0$ for electron-doped compounds, and $\Delta\sigma < 0$ and $\Delta\mathrm{SW} < 0$ for hole-doped compounds. This agrees with previous theoretical calculations using the Boltzmann equation instead of the diagrammatic approach [12,14], as well as with experiments [46,47].

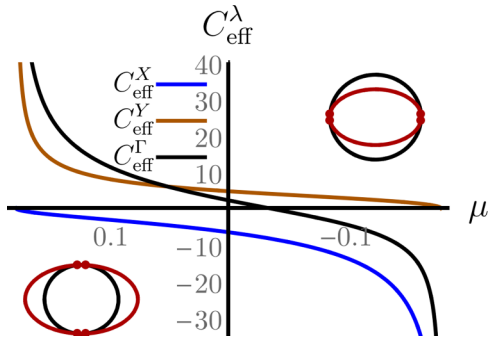

FIG. 4. The coefficient C^{β}_{eff}, as a function of the chemical potential μ (in units of the Fermi energy ϵ_0), for a circular hole pocket at the Γ point and elliptical electron pockets centered at X and Y. The ellipticity here is set to $\delta = 0.35$.

In summary, we studied the impact of anisotropic spin fluctuations on the optical conductivity anisotropy of the nematic phase of iron-based superconductors. Our main result is that, while the DC conductivity anisotropy is determined solely by the collision of electrons and spin fluctuations, the electronic Fermi velocity renormalization induced by spin fluctuations causes opposite changes in the effective scattering rate and plasma frequencies anisotropies that exactly compensate each other in the DC limit. Our results qualitatively agree with recent optical conductivity experiments in detwinned $BaFe_2As_2$. Experimental optical studies of compounds that display nematic order without magnetic order, such as FeSe, would be desirable to further elucidate this unavoidable entanglement between scattering rate and plasma frequency anisotropies in these materials.

We thank fruitful discussions with J. Chu, A. Chubukov, L. Degiorgi, I. Fisher, D. Maslov, and S. Syzranov. M.S. acknowledges the support from the Humboldt Foundation. J.S. acknowledges the support from Deutsche Forschungsgemeinschaft (DFG) through the Priority Program SPP 1458 314 "Hochtemperatur-Supraleitung in Eisenpnioktiden" (Project-No. SCHM 1031/5-1). R.M.F. is supported by the U.S. Department of Energy, Office of Science, Basic Energy Sciences, under Award No. DE-SC0012336.

[1] Y. Ando, K. Segawa, S. Komiya, and A. N. Lavrov, Phys. Rev. Lett. **88**, 137005 (2002).
[2] J.-H. Chu, J. G. Analytis, K. De Greve, P. L. McMahon, Z. Islam, Y. Yamamoto, and I. R. Fisher, Science **329**, 824 (2010).
[3] M. A. Tanatar, E. C. Blomberg, A. Kreyssig, M. G. Kim, N. Ni, A. Thaler, S. L. Bud'ko, P. C. Canfield, A. I. Goldman, I. I. Mazin, and R. Prozorov, Phys. Rev. B **81**, 184508 (2010).
[4] A. Dusza, A. Lucarelli, A. Sanna, S. Massidda, J.-H. Chu, I. R. Fisher, and L. Degiorgi, New J. Phys. **14**, 023020 (2012).
[5] O. Cyr-Choinière, G. Grissonnanche, S. Badoux, J. Day, D. A. Bonn, W. N. Hardy, R. Liang, N. Doiron-Leyraud, and L. Taillefer, Phys. Rev. B **92**, 224502 (2015).
[6] E. Fradkin, S. A. Kivelson, M. J. Lawler, J. P. Eisenstein, and A. P. Mackenzie, Annu. Rev. Condens. Matter Phys. **1**, 153 (2010).

[7] M. Vojta, Adv. Phys. **58**, 699 (2009).
[8] R. M. Fernandes, A. V. Chubukov, and J. Schmalian, Nat. Phys. **10**, 97 (2014).
[9] M. Schütt and R. M. Fernandes, Phys. Rev. Lett. **115**, 027005 (2015).
[10] R. M. Fernandes and J. Schmalian, Supercond. Sci. Technol. **25**, 084005 (2012).
[11] X. Lu, J. T. Park, R. Zhang, H. Luo, A. H. Nevidomskyy, Q. Si, and P. Dai, Science **345**, 657 (2014).
[12] R. M. Fernandes, E. Abrahams, and J. Schmalian, Phys. Rev. Lett. **107**, 217002 (2011).
[13] S. Liang, G. Alvarez, C. Şen, A. Moreo, and E. Dagotto, Phys. Rev. Lett. **109**, 047001 (2012).
[14] M. Breitkreiz, P. M. R. Brydon, and C. Timm, Phys. Rev. B **90**, 121104 (2014).
[15] M. P. Allan, T.-M. Chuang, F. Massee, Y. Xie, N. Ni, S. L. Bud'ko, G. S. Boebinger, Q. Wang, D. S. Dessau, P. C. Canfield, M. S. Golden, and J. C. Davis, Nat. Phys. **9**, 220 (2013).
[16] M. N. Gastiasoro, I. Paul, Y. Wang, P. J. Hirschfeld, and B. M. Andersen, Phys. Rev. Lett. **113**, 127001 (2014).
[17] C.-C. Chen, J. Maciejko, A. P. Sorini, B. Moritz, R. R. P. Singh, and T. P. Devereaux, Phys. Rev. B **82**, 100504 (2010).
[18] W. Lv and P. Phillips, Phys. Rev. B **84**, 174512 (2011).
[19] B. Valenzuela, E. Bascones, and M. J. Calderón, Phys. Rev. Lett. **105**, 207202 (2010).
[20] Z. P. Yin, K. Haule, and G. Kotliar, Nat. Phys. **7**, 294 (2011).
[21] F. Wang, S. A. Kivelson, and D.-H. Lee, Nat. Phys. **11**, 959 (2015).
[22] J. K. Glasbrenner, I. I. Mazin, H. O. Jeschke, P. J. Hirschfeld, R. M. Fernandes, and R. Valenti, Nat. Phys. **11**, 953 (2015).
[23] A. V. Chubukov, R. M. Fernandes, and J. Schmalian, Phys. Rev. B **91**, 201105 (2015).
[24] Y. Yamakawa, S. Onari, and H. Kontani, Phys. Rev. X **6**, 021032 (2016).
[25] A. V. Chubukov, M. Khodas, and R. M. Fernandes, arXiv:1602.05503.
[26] K. Jiang, J. Hu, H. Ding, and Z. Wang, Phys. Rev. B **93**, 115138 (2016).
[27] W. Götze and P. Wölfle, Phys. Rev. B **6**, 1226 (1972).
[28] D. N. Basov and T. Timusk, Rev. Mod. Phys. **77**, 721 (2005).
[29] C. Mirri, A. Dusza, S. Bastelberger, M. Chinotti, L. Degiorgi, J.-H. Chu, H.-H. Kuo, and I. R. Fisher, Phys. Rev. Lett. **115**, 107001 (2015).
[30] R. M. Fernandes, A. V. Chubukov, J. Knolle, I. Eremin, and J. Schmalian, Phys. Rev. B **85**, 024534 (2012).
[31] A. Sanna, F. Bernardini, G. Profeta, S. Sharma, J. K. Dewhurst, A. Lucarelli, L. Degiorgi, E. K. U. Gross, and S. Massidda, Phys. Rev. B **83**, 054502 (2011).
[32] K. Sugimoto, E. Kaneshita, and T. Tohyama, J. Phys.: Conf. Ser. **400**, 022113 (2012).
[33] L. Benfatto, E. Cappelluti, L. Ortenzi, and L. Boeri, Phys. Rev. B **83**, 224514 (2011).
[34] X. Zhang and E. Dagotto, Phys. Rev. B **84**, 132505 (2011).
[35] G. Derondeau, S. Polesya, S. Mankovsky, H. Ebert, and J. Minár, Phys. Rev. B **90**, 184509 (2014).
[36] S. V. Syzranov and J. Schmalian, Phys. Rev. Lett. **109**, 156403 (2012).
[37] D. S. Inosov, J. T. Park, P. Bourges, D. L. Sun, Y. Sidis, A. Schneidewind, K. Hradil, D. Haug, C. T. Lin, B. Keimer, and V. Hinkov, Nat. Phys. **6**, 178 (2010).
[38] S. O. Diallo, D. K. Pratt, R. M. Fernandes, W. Tian, J. L. Zarestky, M. Lumsden, T. G. Perring, C. L. Broholm, N. Ni, S. L. Bud'ko, P. C. Canfield, H.-F. Li, D. Vaknin, A. Kreyssig, A. I. Goldman, and R. J. McQueeney, Phys. Rev. B **81**, 214407 (2010).
[39] G. S. Tucker, R. M. Fernandes, H.-F. Li, V. Thampy, N. Ni, D. L. Abernathy, S. L. Bud'ko, P. C. Canfield, D. Vaknin, J. Schmalian, and R. J. McQueeney, Phys. Rev. B **86**, 024505 (2012).
[40] A. Abanov, A. V. Chubukov, and J. Schmalian, Adv. Phys. **52**, 119 (2003).
[41] See Supplemental Material at http://link.aps.org/supplemental/10.1103/PhysRevB.94.075111, which includes Refs. [9] and [42], for (i) the calculational details of C_{eff}^{β}, (ii) a general Kramers-Kronig based argument on the entanglement of the signs of $\Delta\tau^{-1}$ and $\Delta\lambda$, (iii) the estimation of impurity scattering and (iv) an illustration of the theoretically predicted regime, that is expected to be observable in optical experiments.
[42] D. C. Johnston, Adv. Phys. **59**, 803 (2010).
[43] A detailed study of the isotropic AC conductivity in this limit will be reported elsewhere.
[44] C. Liu, A. D. Palczewski, R. S. Dhaka, T. Kondo, R. M. Fernandes, E. D. Mun, H. Hodovanets, A. N. Thaler, J. Schmalian, S. L. Bud'ko, P. C. Canfield, and A. Kaminski, Phys. Rev. B **84**, 020509 (2011).
[45] I. Eremin and A. V. Chubukov, Phys. Rev. B **81**, 024511 (2010).
[46] E. C. Blomberg, M. A. Tanatar, R. M. Fernandes, I. I. Mazin, B. Shen, H.-H. Wen, M. D. Johannes, J. Schmalian, and R. Prozorov, Nat. Commun. **4**, 1914 (2013).
[47] H.-H. Kuo, J.-H. Chu, S. A. Kivelson, and I. R. Fisher, Science **352**, 958 (2016).